

# FBNet: Feature Balance Network for Urban-Scene Segmentation

Lei Gan<sup>\*1</sup>, Huabin Huang<sup>\*2</sup>, Banghuai Li<sup>2</sup>, Ye Yuan<sup>2</sup>

<sup>1</sup> Beihang University <sup>2</sup> MEGVII Technology  
ganlei@buaa.edu.cn, {huanghuabin, libanghuai, yuanye}@megvii.com

## Abstract

Image segmentation in the urban scene has recently attracted much attention due to its success in autonomous driving systems. However, the poor performance of concerned foreground targets, e.g., traffic lights and poles, still limits its further practical applications. In urban scenes, foreground targets are always concealed in their surrounding stuff because of the special camera position and 3D perspective projection. What's worse, it exacerbates the unbalance between foreground and background classes in high-level features due to the continuous expansion of the reception field. We call it *Feature Camouflage*. In this paper, we present a novel add-on module, named **Feature Balance Network (FBNet)**, to eliminate the feature camouflage in urban-scene segmentation. FBNet consists of two key components, i.e., *Block-wise BCE (BwBCE)* and *Dual Feature Modulator (DFM)*. BwBCE serves as an auxiliary loss to ensure uniform gradients for foreground classes and their surroundings during backpropagation. At the same time, DFM intends to enhance the deep representation of foreground classes in high-level features adaptively under the supervision of BwBCE. These two modules facilitate each other as a whole to ease feature camouflage effectively. Our proposed method achieves a new state-of-the-art segmentation performance on two challenging urban-scene benchmarks, i.e., *Cityscapes* and *BDD100K*. Code will be released for reproduction.

## 1. Introduction

Semantic image segmentation, a fundamental task in computer vision, is widely employed in basic urban-scene understanding scenarios such as autonomous driving, image editing, etc. With the recent development of convolutional neural network-based methods [35, 20, 23, 26, 42, 44], urban-scene segmentation has achieved great improvement. However, almost all these methods ignore the data distribution characteristics of the urban scene and treat it as a

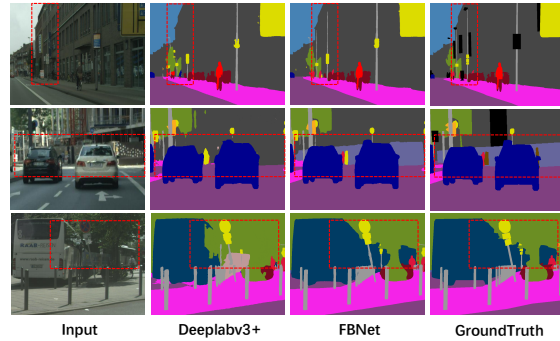


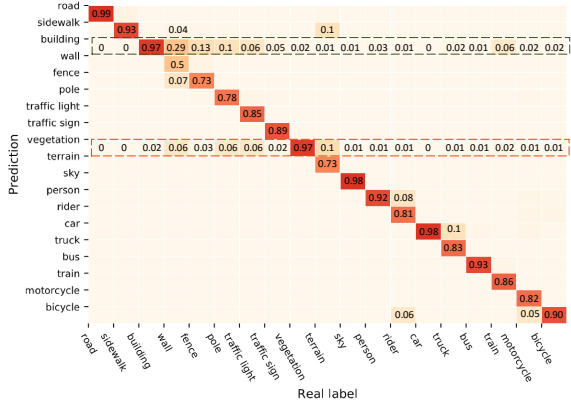
Figure 1. Segmentation results based on DeepLabv3+ [7]. Obvious improvements over DeepLabv3+ are marked in red dashed boxes. Our proposed FBNet distinguishes poles, wall, and bus pixels from their surrounding effectively.

common segmentation task. The performance of many important targets is still limited, and the reason hasn't been fully exploited, which restricts its further application.

As shown in Figure 2 (b), foreground targets like lamp poles are always concealed by surrounding background stuff like buildings due to the camera's special position and 3D perspective projection. Consequently, these foreground targets usually tend to be misclassified as their surrounding stuff by many state-of-the-art (SOTA) semantic segmentation works. We take DeepLabv3+ [7] as an example and obtain its confusion matrix between each class pair on Cityscapes [14] validation dataset in Figure 2 (a). We can find that about 29% wall and 13% fence pixels are misclassified as buildings. We delve into this phenomenon and ascribe it to two reasons. First, background stuff<sup>1</sup> always occupy much more pixels than foreground targets in urban-scene images. Thus, foreground classes will contribute less to backpropagated gradients during model optimization, which results in a model bias towards background stuff classes. It is known widely as *Class Imbalance (Gradient Imbalance)* problem. Second, deep convolutional neural networks in semantic segmentation rely on high-level discriminative features to distinguish each class accurately.

<sup>1</sup>We define road, sidewalk, building, sky and vegetation as the background stuff in this paper, because all of them tends to occupy main area of the image and is widely adopted as background in practical urban-scene applications [14, 51], and the other classes we call foreground classes.

\*These authors contributed equally



(a)



(b)

Figure 2. Observations on Cityscapes [14] validation dataset. (a) Confusion matrix of DeepLabv3+ [7]. We can find that many foreground target pixels are misclassified as buildings or vegetation, e.g. 29% wall and 13% fence pixels are misclassified as buildings. (b) Examples of foreground classes, which are highlighted in red and green dashed boxes.

However, high-level features are always achieved by a series of reception field expansion operations like convolution and dilated convolution, which leads to the continuous dilution of foreground target features by the surrounding background stuff. Finally, it exacerbates the unbalance between foreground and background classes in high-level feature maps. We call it *Feature Camouflage*. Figure 3 illustrates this issue intuitively. Several attempts [7, 31, 29, 43, 29, 11] focus on fusing low-level features with high-level features may ease the problem implicitly, but high-level features are more discriminative [56, 33, 58, 32] and still dominate the final classification.

Although many methods like loss re-weighting [15, 2, 22, 41] and data over-sampling [46, 4, 17, 19, 61] have been proposed to relieve the class imbalance. We argue that these methods have a very limited impact on the feature camouflage problem. They only utilize the pixel number statistics of images or labels to balance the overall performance, while the essential analysis on the high-level features is sel-

dom exploited. In this paper, we propose a novel Feature Balance Network (FBNet) as an add-on module to solve the feature camouflage problem by exploring the spatial relationship between foreground classes and background stuff classes. FBNet aims to balance the high-level feature explicitly and highlights more foreground targets from their surrounding stuff. It consists of two key components, i.e., Block-wise Binary Cross-Entropy (BwBCE) and Dual Feature Modulator (DFM).

BwBCE serves as an auxiliary loss to enhance the representation of foreground classes in the deep layers to ease the feature camouflage problem. As we all know, point-wise cross-entropy is widely adopted in the past semantic segmentation works to achieve the analogous purpose. However, point-wise cross-entropy only concentrates on the single pixel to classify it into the correct class. Obviously, if some class occupies the most pixels, it will dominate the model optimization due to the cumulative effect, while the scarce target class will be suppressed correspondingly. In contrast, our proposed BwBCE is designed from a gradient balanced perspective. BwBCE treats all pixels belonging to the same class as a whole to ensure uniform gradient for the foreground class and its surroundings during backpropagation. It highlights the existence of foreground class in the high-level features and obtains a more robust feature representation for foreground classes.

According to the above discussion, BwBCE tends to cause potential conflict with the final segmentation loss, which is a typical point-wise cross-entropy loss, if we combine them together to supervise the model training directly. For this reason, we propose a flexible yet effective module named DFM to make them work in a more proper way. DFM consists of two main components, i.e., channel sensor and spatial sensor. These two modules attempt to strengthen the feature representation of foreground classes from the channel and spatial dimension respectively under the full supervision of BwBCE. Then, fusing the output feature of DFM with the original one will solve the feature camouflage problem effectively and boost the overall performance.

It is worth mentioning that our proposed FBNet is orthogonal with the existing SOTA methods. Methods equipped with our approach can achieve further improvements with negligible cost, verified in Section 4.2. Apart from this, we conduct extensive experiments in Section 4 to prove each component’s effectiveness in FBNet. Superior performance on two challenging urban-scene segmentation benchmarks, i.e., Cityscapes [14] and BDD100K [51], shows the effectiveness and robustness of our proposed method as well. In summary, the contributions of this paper are three-fold:

- We delve into the poor performance of foreground classes in the urban-scene segmentation and attribute it to feature camouflage empirically, which is seldom

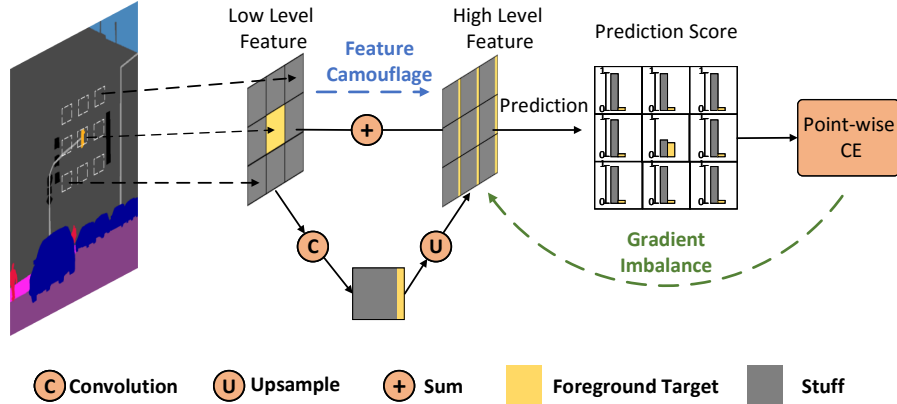


Figure 3. Illustration of feature camouflage. High-level features are always achieved by a series of reception field expansion operations like convolution and dilated convolution, which leads to the continuous dilution of foreground targets’ features by the surrounding stuff. For example, the feature of *lamp* is diluted by its surrounding background stuff *building* in this figure. Thus, the *lamp* is under-represented and results in poor performance. We call this phenomenon *Feature Camouflage*.

exploited in the past works.

- We propose a novel module named Feature Balance Network(FBNet), which consists of two key components, i.e., Block-wise Binary Cross-Entropy (Bw-BCE) and Dual Feature Modulator(DFM), to ease the feature camouflage effectively.
- Our proposed method can achieve superior performance over all the SOTA methods on two challenging urban-scene benchmarks [14, 51], especially on foreground categories.

## 2. Related Work

**Semantic Segmentation** Semantic Segmentation is a fundamental visual task aiming at setting class label for every pixel of the image. Maintaining the resolution of a feature map while capturing discriminative high-level features is vital important for high performance of semantic segmentation. Usually, high-level features are extracted by some continuous downsample convolutions and spatial pooling layers, but the resolution gets coarser in the procedure because of the growing reception field. Several researches [35, 38] relieve this problem by leveraging deconvolution for learnable upsampling from low-resolution features. Some more intuitive and effective method [1, 39, 30, 7] hire skip-connections to maintain high-resolution and discriminative fused feature to recover the object boundaries. Another prevalent method is atrous convolution [5, 50], which increases the receptive field size while keeping resolution without increasing the number of parameters, and it is widely adopted in recent semantic segmentation networks [6, 7, 47, 55, 60]. Additionally, ASPP [6] and pyramid pooling modules [57] address such challenges caused by diverse scales of objects.

**Urban-scene Exploitation** In the field of urban-scene

parsing, several studies exploit the urban-scene images characteristics. In general, the scale of targets significantly vary in the urban-scene images. FoveaNet [27] localizes a “fovea region”, where the small scale objects are crowded, and performs scale normalization to address heterogeneous object scales. Another recent approach [60] exploits the fact that the urban-scene images have continuous video frame sequences and proposes the data augmentation technique based on a video prediction model to create future frames and their labels. HANet [12] emphasizes informative features or classes selectively according to the vertical position of a pixel. Another approach [10] separates an urban-scene image into several spatial regions and conducts domain adaptation on the pixel-level features from the same spatial region.

**Class Imbalance** In urban-scene images, few categories occupy most pixels which results minority classes can not get enough gradient during training strategy. Thus, the performance of minority classes is often not as good as majority classes. This is the widely studied class imbalance problem. Many approaches have been proposed to deal with class imbalance. Some use re-sampling strategies [4, 17, 19, 61] to re-balance data distribution. In their basic versions, the dataset is balanced by increasing the number of objects from “minority” classes, respectively. But over-sampling methods tend to over-fit due to the inclusion of duplicate data. Re-weighting [15, 2, 22] is another widely used approach. It assigns each category different weights according to the points number to simply increase minority classes gradient. All these methods only care about points number of different targets but do not take into account the positional relationship between them, which limits their ability to refine weak target segmentation.

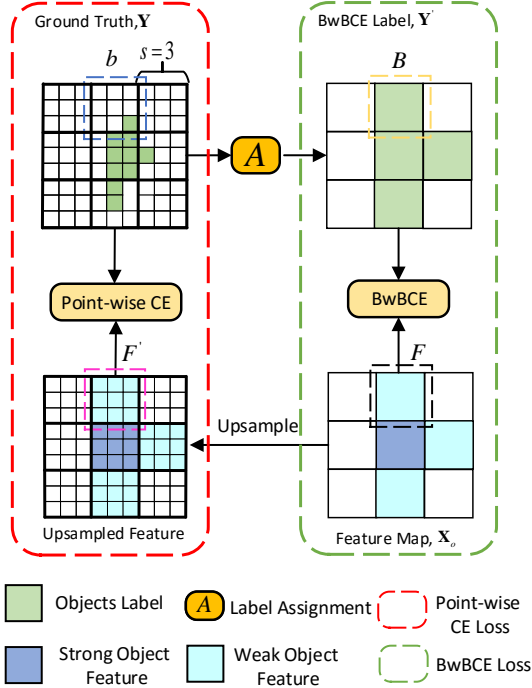


Figure 4. Illustration of difference between BwBCE and Point-wise cross-entropy.  $s$  is the stride of high-level feature maps,  $Y$  is the the ground-truth label mask.  $A$  means the label assignment process to convert  $Y$  into  $Y'$  to match the output size of  $X_o$ .  $F$  in high level feature map is weak foreground target feature because of feature camouflage. The feature points in dash box  $F'$  are up-sampled from  $F$ .

### 3. Proposed Method

In this paper, we propose a novel method named Feature Balance Network (FBNet) from feature manipulation perspective. It consists of two key components, i.e., Block-wise Binary Cross-Entropy(BwBCE) Loss and Dual Feature Modulator(DFM). FBNet intends to enhance foreground high-level features to relieve the feature camouflage problem. An overview of our pipeline can be found in Figure 5. In the following section, we will illustrate BwBCE and DFM respectively, followed by the details in training objective and network architecture.

#### 3.1. Block-wise Binary Cross Entropy Loss

FBNet intends to strengthen the deep representation of foreground classes in high-level features. Thus, the fundamental factor is to perceive where to perform the optimization. In this section, we design a simple but effective auxiliary loss named Block-wise Binary Cross-Entropy (BwBCE) loss to achieve the goal.

In fact, introducing auxiliary loss for robust feature learning in deep layers is a common strategy in semantic segmentation [13]. However, almost all these meth-

ods [57, 55, 3, 49] adopt the point-wise cross-entropy as the auxiliary loss, which has no difference with the final classification loss. Point-wise, cross-entropy has the inherent drawback towards the feature camouflage problem. As shown in Figure 4, high-level feature maps are always up-sampled to the size of the label mask, then each corresponding pixel pair in the feature map and label mask is used to calculate the cross-entropy loss. Assuming  $F \in \mathbb{R}^{1 \times 1}$  is one single pixel in the high-level feature map (bottom-right corner in Figure 4),  $F$  will be 3x upsampled to  $F' \in \mathbb{R}^{3 \times 3}$  to match the size of label mask. If only one pixel in  $F'$  is marked as foreground class in the label mask (top-left corner in Figure 4), merely 1/9 of the gradient in  $F'$  contributes to the foreground class optimization during backpropagation, which harms the foreground class feature presentation due to the gradient dilution.

On the contrary, our proposed BwBCE is designed to ease feature camouflage explicitly from a gradient perspective. As shown in Figure 5,  $P \in \mathbb{R}^{C \times h \times w}$  is the prediction result,  $\hat{C}$  is the number of foreground classes,  $Y \in \mathbb{R}^{H \times W}$  is the ground-truth label mask.  $A$  means the label assignment to convert  $Y$  into  $Y' \in \mathbb{R}^{C \times h \times w}$ , and  $Y'$  is in a multi-hot format which serves as the direct supervision of  $P$ . Formally,  $A$  is defined as follows:

$$Y' = A(Y) \quad (1)$$

and

$$Y'_{c,i,j} = \varepsilon \left( \sum_{k=s \cdot i}^{s \cdot (i+1)} \sum_{l=s \cdot j}^{s \cdot (j+1)} Y_{k,l} = c \right) \quad (2)$$

where  $c \in [0, \hat{C}]$ ,  $i \in [0, h)$ ,  $j \in [0, w)$ ,  $s = \frac{H}{h}$  or  $s = \frac{W}{w}$  is the stride of  $P$ ,  $\varepsilon(x) = 1$  if  $x \geq 0$  and 0 otherwise. In a nutshell, if any pixel of class  $c$  falls on block  $b \in Y^{s \times s}$ , the corresponding position of multi-hot vector in  $Y'$  will be set 1 else 0, as shown in Figure 4. In addition,  $P$  is defined as follows:

$$P = \sigma(G_{conv}(X_o)) \quad (3)$$

$\sigma$  stands for the *sigmoid* function,  $G_{conv}$  is a typical convolution operation, and  $X_o$  is the input high-level features. Ultimately, our proposed BwBCE loss can be described as:

$$L_{BwBCE}(P, Y') = \sum_{c=0}^{\hat{C}} \sum_{i=0}^h \sum_{j=0}^w Y'_{c,i,j} \cdot \log P_{c,i,j} + (1 - Y'_{c,i,j}) \cdot \log(1 - P_{c,i,j}) \quad (4)$$

Comparing our BwBCE with point-wise cross-entropy, the main difference lies in that BwBCE ensures uniform gradient for foreground class and its surroundings during backpropagation even if huge pixel imbalance exists between them, while point-wise cross-entropy tends to result in serious gradient dilution for scarce foreground class. What's more, even loss re-weighting strategies is adopted to

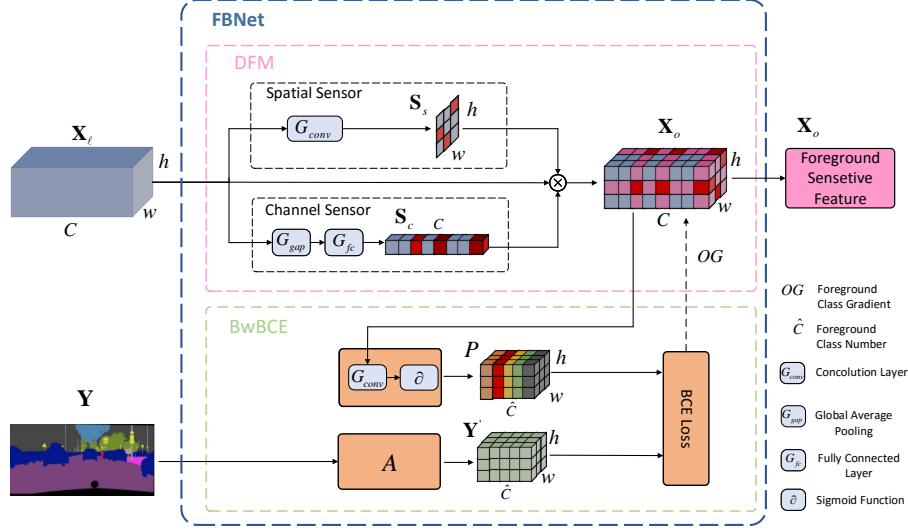


Figure 5. Architecture of our proposed FBNet. FBNet is composed of two main parts, DFM and BwBCE. DFM applies spatial and channel sensor on the original feature  $\mathbf{X}_\ell$  to get spatial weight  $\mathbf{S}_s$  and channel weight  $\mathbf{S}_c$  respectively. Then, output features  $\mathbf{X}_o$  can be obtained by fusing  $\mathbf{S}_s$ ,  $\mathbf{S}_c$  with  $\mathbf{X}_\ell$ . BwBCE compels  $\mathbf{X}_o$  to preserve more foreground target features during the training procedure. The key factor label generator  $A$  generates the foreground target label  $\mathbf{Y}'$  from original label  $\mathbf{Y}$ . Details can be found in Section 3.2.

point-wise cross-entropy is incapable of solving this problem. Thus, BwBCE is more suitable as the auxiliary loss for more balance feature learning.

### 3.2. Dual Feature Modulator

Generally speaking, point-wise cross-entropy loss is widely adopted for the final classification to distinguish each pixel in the semantic segmentation. However, BwBCE just focuses on enhancing the representation of scarce foreground class in high-level features, which goes against the fine-grained classification to some extent as we have discussed in Section 3.1. It may tend to arouse inconsistent optimization objectives when we combine them as a whole to supervise the same features blindly.

To avoid the potential conflict, we design a flexible yet effective module named *Dual Feature Modulator*(DFM). DFM transforms the given features under the full supervision of BwBCE loss, which is independent of the point-wise cross-entropy for the final classification. Thereby, the output of DFM achieves better feature representation for the foreground class. Mixing the transformed features with the original ones will contribute to the final performance. Several visualization examples shown in Figure 7 can illustrate the effectiveness of DFM intuitively.

As shown in Figure 5, DFM is designed on both channel and spatial dimensions. We summarize them as **Channel Sensor** and **Spatial Sensor** respectively. The channel sensor plays an important role in identifying which channel is more important for foreground targets' segmentation, while the spatial sensor intends to perceive the specific location of

the foreground targets. Their outputs,  $\mathbf{S}_s$  and  $\mathbf{S}_c$ , are defined as follows:

$$\mathbf{S}_s = \sigma(G_{conv}(\mathbf{X}_\ell)) \quad (5)$$

$$\mathbf{S}_c = \sigma(G_{fc}(G_{pool}(\mathbf{X}_\ell))) \quad (6)$$

$G_{conv}$  is a  $1 \times 1$  convolution operation,  $G_{pool}$  is a global average pooling operation, and  $G_{fc}$  is a fully connected layer.  $\sigma$  is the sigmoid function to normalize  $\mathbf{S}_s$  and  $\mathbf{S}_c$  between 0 and 1. Eventually, the output feature map  $\mathbf{X}_o$  can be described as:

$$\mathbf{X}_o = \mathbf{X}_\ell \otimes G_{bro}(\mathbf{S}_s) \otimes G_{bro}(\mathbf{S}_c) \quad (7)$$

$\otimes$  means points-wise multiplication.  $G_{bro}$  is a broadcast operation to ensure  $\mathbf{S}_s$  and  $\mathbf{S}_c$  have the same shape with  $\mathbf{X}_\ell$ . As a result,  $\mathbf{X}_o$  is supposed to benefit to foreground classes in feature representation. In the end, we fuse  $\mathbf{X}_o$  with  $\mathbf{X}_\ell$  to modulate the deep representation adaptively during the model training.

It is worth noting that BwBCE and DFM are designed as a whole to facilitate each other. Extensive experiments in Section 4.2 can well verify the relationship between them.

### 3.3. Training Objectives

The overall loss of our proposed method is

$$L = \lambda_1 \sum_{f=1}^F L_{BwBCE}(\mathbf{P}, \mathbf{Y}') + \lambda_2 L_{ce}(\mathbf{Z}, \mathbf{Y}) \quad (8)$$

Method	Backbone	mIoU	f-mIoU	road	swalk	build.	veg	sky	wall	fence	pole	tigh.	tsign.	terr.	pers.	rider	car	truck	bus	train	mcyc	bcyc
FCN +Ours	ResNet-50	76.3	70.5	98.0	84.4	92.4	<b>92.7</b>	94.6	47.0	59.0	66.7	73.4	80.3	61.2	82.8	63.0	94.7	62.3	83.0	71.0	63.5	78.9
		<b>78.5</b>	<b>73.4</b>	<b>98.2</b>	<b>85.6</b>	<b>92.9</b>	<b>92.7</b>	<b>94.8</b>	<b>55.4</b>	<b>61.1</b>	<b>67.5</b>	<b>74.4</b>	<b>81.3</b>	<b>62.7</b>	<b>83.5</b>	<b>63.9</b>	<b>95.5</b>	<b>72.8</b>	<b>89.1</b>	<b>76.2</b>	<b>64.9</b>	<b>79.6</b>
FCN +Ours	ResNet-101	77.8	72.4	<b>98.4</b>	<b>86.6</b>	93.1	92.8	95.1	56.0	62.5	68.9	74.1	82.1	64.6	83.9	65.3	95.0	62.6	84.2	66.9	67.5	79.4
		<b>80.7</b>	<b>76.2</b>	98.2	86.0	<b>93.5</b>	<b>93.1</b>	<b>95.3</b>	<b>62.9</b>	<b>63.7</b>	<b>69.6</b>	<b>75.0</b>	<b>82.7</b>	<b>65.2</b>	<b>84.5</b>	<b>66.7</b>	<b>95.7</b>	<b>77.4</b>	<b>89.3</b>	<b>84.5</b>	<b>69.8</b>	<b>80.1</b>

Table 1. Fine-grained segmentation results on the Cityscapes *validation* set. Dilated FCN [50] is adopted as the baseline to evaluate on both ResNet-50 and ResNet-101 backbones. Note that our method improves all foreground categories which are marked in blue.

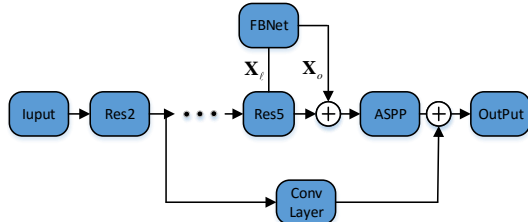


Figure 6. Semantic segmentation networks incorporating FBNet. FBNet generates feature map  $X_o$  which is rich in foreground targets feature, then original feature map  $X_l$  and  $X_o$  will be fused to generate new high level feature map.

$L_{ce}$  is the typical cross-entropy loss for segmentation,  $\mathbf{Z}$  is the final classification score map, and  $\mathbf{Y}$  is the corresponding pixel annotations.  $\lambda_1$  and  $\lambda_2$  are loss weight hyper-parameters to balance the scale of the losses, which we set both 1 as default.

### 3.4. Network architecture

Figure 6 illustrates the overall pipeline of our proposed FBNet based on the SOTA model DeepLabv3+ [7]. FBNet is designed as a plug-and-play module to insert into any layer from Res2 to Res5. Moreover, we conduct extensive ablation studies in Section 4.2 to determine the performance gain by adding FBNet into different layers.

## 4. Experiments

In this section, we first introduce two typical urban-scene segmentation datasets, i.e., Cityscapes[14] and Berkeley Deep Drive dataset (BDD100K)[51], followed by our training protocols. Then we conduct quantitative ablation studies on multiple backbones (e.g. ResNet-50 [20] and ResNet-101 [20]) and several different architectures (e.g. FCN [35], PSPNet [57] and DeepLabv3+ [7]) to demonstrate the effectiveness and wide applicability of our proposed methods. Furthermore, we visualize the feature map generated by FBNet to verify the effect of FBNet intuitively.

We follow standard settings [25, 54, 49, 24, 52, 48] to measure the segmentation performance in terms of the **mean Intersection over Union (mIoU)** metric. Particularly, for the performance evaluation on foreground classes, we adopt the f-mIoU metric, which stands for mIoU of foreground classes.

### 4.1. Datasets and training protocols

**Cityscapes** [14] is a large urban-scene dataset, which has 5000 finely annotated images and 20000 coarsely annotated images. The finely annotated data is split into 2975 training images, 500 validation images, and 1525 testing images. The whole dataset has 19 classes for semantic segmentation, and the image size is  $1024 \times 2048$  by default.

**Berkeley Deep Drive dataset (BDD100K)** [51] is a large urban-scene dataset consisting of 7,000 training and 1,000 validation images for semantic segmentation. The resolution of each image is  $1280 \times 720$ . It's really challenging because it covers various scenes including day, night and diverse weather conditions.

**Implementation Details.** We use SGD with momentum 0.9 and weight decay  $1e-4$  for optimization. The poly schedule [34] is used to decay the learning rate which means the initial learning rate is multiplied by  $(1 - \frac{iter}{max.iter})^{0.9}$ . We set the initial learning rate as 0.01 and the power as 0.9. We train the model for 180 epochs and on both Cityscapes and BDD100K with a batch size of 8. During model training, we perform random resizing with a scale range in [0.5, 2.0], random flipping and random cropping with a crop size of  $832 \times 832$  on the input images. It is worth noting that results reported in this paper are based on a sliding window with a single scale across the whole image unless explicitly specified. In addition, we adopt a strong baseline with OHEM [40], data oversampling and loss re-weighting strategies, which are always used towards gradient imbalance as our basic model. We conduct all experiments on a machine with 8 2080Ti GPUs, which minimizes the barriers to make all our results easy to reproduce.

### 4.2. Ablation studies

**Ablation for different backbones.** We take Dilated FCN [50] as our baseline model to evaluate FBNet based on two classic backbones, i.e., ResNet-50 [20] and ResNet-101 [20]. Detailed results on Cityscapes *validation* set are listed in Table 1. It is obvious that Dilated FCN with FBNet achieves significant improvements over corresponding baselines on both ResNet-50 and ResNet-101 backbones. For example, FBNet based on ResNet-101 can boost overall segmentation performance from 77.8% to 80.7% on mIoU and from 72.4% to 76.2% on f-mIoU, which achieves about 2.9% and 3.8% improvements respectively.

**Ablation over different state-of-the-art methods.** Our motivation is to design FBNet as a plug-and-play module. Thus, we integrate FBNet with several strong SOTA models like PSPNet [57] and DeepLabv3+ [7] to verify the effectiveness of FBNet. We can find from Table 2 that FBNet achieves up to **1.2%** and **1.7%** improvements on mIoU and f-mIoU respectively. In addition, we also report the total FLOPs of each model based on  $1024 \times 1024$  resolution for a more clear comparison. Our FBNet only increases 0.76 GFLOPs (around **0.1%**) over PSPNet and DeepLabv3+, which indicates that FBNet can be widely adopted to any SOTA frameworks to achieve further improvements with negligible cost.

Method	mIoU	$\Delta$	f-mIoU	$\Delta$	GFLOPs
PSPNet [57]	79.3	-	74.5	-	540.78
DeepLabv3+ [7]	79.5	-	74.7	-	760.44
<b>Ours+PSPNet</b>	<b>80.5</b>	<b>1.2<math>\uparrow</math></b>	<b>76.2</b>	<b>1.7<math>\uparrow</math></b>	541.54
<b>Ours+DeepLabv3+</b>	<b>80.6</b>	<b>1.1<math>\uparrow</math></b>	<b>76.1</b>	<b>1.4<math>\uparrow</math></b>	761.20

Table 2. Ablation over different SOTA methods, where ResNet-50 serves as the backbone. The GFLOPs are computed based on  $1024 \times 1024$  resolution.

**Ablation for the proper layer to inject FBNet.** In this section, we conduct extensive experiments to explore the proper layer (from Res2 to Res5) to inject our FBNet. As we can see from Table 3, no matter where we inject FBNet, it can obtain consistent improvements and maximum is achieved when FBNet is plugged in the deepest layer. However, it is noteworthy that if we inject FBNet to all the layers or the deepest layer, they actually achieve almost the same results. In fact, it is in line with our expectations as high-level layers suffer from a more serious feature camouflage problem due to the continuous expansion of the receptive field, which exactly satisfies our assumption in Section 1.

Method	Res2	Res3	Res4	Res5	mIoU	f-mIoU
Baseline	-	-	-	-	77.8	70.6
+FBNet	$\checkmark$				78.7	73.6
		$\checkmark$			79.5	74.6
			$\checkmark$		80.1	75.4
				$\checkmark$	80.7	76.2
	$\checkmark$	$\checkmark$	$\checkmark$	$\checkmark$	<b>80.8</b>	<b>76.3</b>

Table 3. Ablation on the proper layer to inject FBNet. Res2  $\sim$  Res5 mean the different stages in Dilated FCN [50] with ResNet-101 backbone.

**Ablation on each component of FBNet.** As we have discussed in Section 3, FBNet consists of two key components, i.e., BwBCE and DFM. Thus, we conduct comprehensive experiments from auxiliary loss and feature modulator perspectives to verify the superiority of our proposed compo-

nents in FBNet. As shown in Table 4, even if we only adopt one of BwBCE and DFM into the baseline model, it can achieve about **0.9%** and **1.2%** improvements respectively. Apart from this, we combine the different choices of auxiliary loss and feature modulator together to clarify the impact of each component. We can find that although point-wise cross-entropy and  $1 \times 1$  convolution can boost the segmentation performance, FBNet equipped with BwBCE and DFM can obtain further improvements (up to **2.9%**) beyond them. Another minor details should be emphasized that these two modules, i.e., BwBCE and DFM, can facilitate each other (**2.9% > 0.9% + 1.2%**), which keeps consistent with our discussion in Section 3. BwBCE and DFM should be treated as a whole to enhance the feature representation of foreground classes.

Component	Auxiliary Loss		FM		mIoU	$\Delta$
	P-CE	BwBCE	Conv	DFM		
Baseline	-	-	-	-	77.8	-
FBNet		$\checkmark$			78.7	<b>0.9<math>\uparrow</math></b>
				$\checkmark$	79.0	<b>1.2<math>\uparrow</math></b>
	$\checkmark$			$\checkmark$	80.0	<b>2.2<math>\uparrow</math></b>
		$\checkmark$	$\checkmark$		79.4	<b>1.6<math>\uparrow</math></b>
FBNet	-	$\checkmark$	-	$\checkmark$	<b>80.7</b>	<b>2.9<math>\uparrow</math></b>

Table 4. Ablation on each component of FBNet, where Dilated FCN [50] with the ResNet-101 serves as the baseline. P-CE means point-wise Cross Entropy Loss, Conv means  $1 \times 1$  convolution, FM means feature modulator.

### 4.3. Comparison with state-of-the-art methods

**Results on Cityscapes test set.** For a fair and complete comparison with the SOTA methods, we train our models under several different configurations, i.e., only finely annotated data is accessible, extra coarsely annotated data is added, model is initialized with Mapillary pre-trained model. Moreover, we follow the standard settings in [18, 57, 54, 24, 48, 49] to adopt multi-scale and flipping testing strategies. As shown in Table 5, our proposed FBNet achieves **82.4%** mIoU with ResNet101 backbone and **83.9%** mIoU with WiderResNet38 [53], Mapillary [37] pre-trained model and coarse training dataset, which sets up a new SOTA result.

**Results on BDD100K.** To further verify the effect of our proposed method, we evaluate our method on another challenging urban-scene dataset, i.e., BDD100K, based on the DeepLabv3+ [7]. Table 6 shows the detailed results. Obviously, our method also achieves SOTA performance. Comparing with the DeepLabv3+ baseline, FBNet improves the mIoU from **64.91%** to **66.3%** on the single scale inference without flipping, which demonstrates the effectiveness of our FBNet.

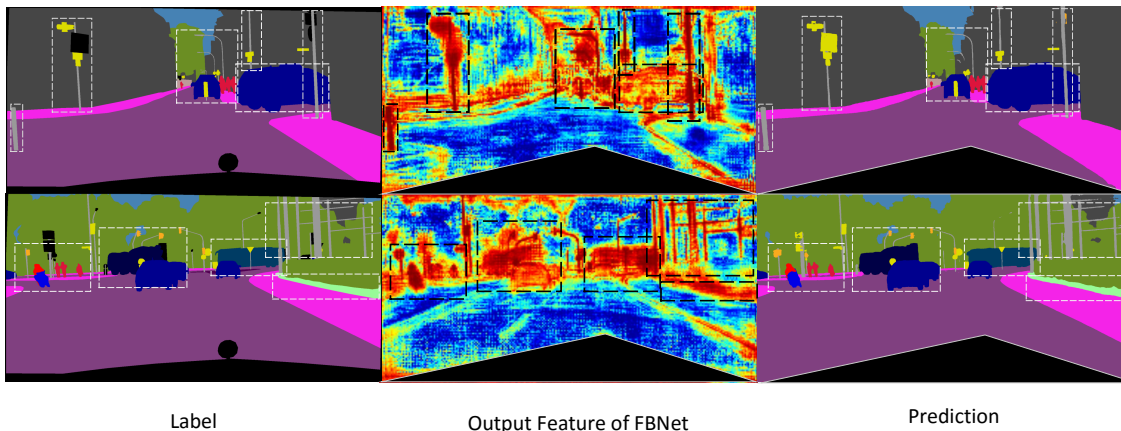


Figure 7. : Visualization of FBNet output feature map. We do reduction mean along channel dimension, the feature intensity gradually increases from blue to red, for better visualization, we hide the ignored area. It can be easily noticed that the foreground targets feature are much stronger than background stuff feature. Thus adding this feature map back to the original feature map can relieve feature camouflage.

Method	Conference	Backbone	mIoU(%)
PSPNet[57]	CVPR 2017	ResNet-101	78.4
DFN[50]	ICLR 2016	ResNet-101	79.3
AAF[25]	ECCV 2018	ResNet-101	80.1
DenseASPP[47]	CVPR 2018	DenseNet-161	80.6
CPNet [48]	CVPR 2020	ResNet-101	81.3
BFP[16]	ICCV 2019	ResNet-101	81.4
DANet [18]	CVPR 2019	ResNet-101	81.5
CCNet [24]	ICCV 2019	ResNet-101	81.4
SpyGR [28]	CVPR 2020	ResNet-101	81.6
ACFNet [54]	ICCV 2019	ResNet-101	81.8
OCR [52]	ECCV 2020	ResNet-101	81.8
CDGCNet [21]	ECCV 2020	ResNet-101	82.0
HANet [12]	CVPR 2020	ResNet-101	82.1
RecoNet [9]	ECCV 2020	ResNet-101	82.3
QCO [59]	CVPR 2021	ResNet-101	82.3
<b>Ours</b>	N/A	ResNet-101	<b>82.4</b>
DeepLabv3+ <sup>†</sup> [7]	ECCV 2018	Xception	82.1
SpyGR <sup>†</sup> [28]	CVPR 2020	ResNet-101	82.3
GSCNN <sup>‡</sup> [45]	ICCV 2019	WiderResNet38	82.8
HANet <sup>†‡</sup> [12]	CVPR 2020	ResNext-101	83.2
<b>Ours<sup>†‡</sup></b>	N/A	WiderResNet38	<b>83.9</b>

Table 5. Performance comparisons on the Cityscapes *test* set. <sup>†</sup> means Cityscapes coarsely annotated images are adopted for model training. <sup>‡</sup> means model is initialized by Mapillary pre-trained model.

#### 4.4. Visual inspections and analysis

**Visualization of segmentation results.** As shown in Figure 1, we take DeepLabv3+ [7] as baseline to compare segmentation results with ours. It is obvious that FBNet distinguishes more foreground targets from its surrounding,

which is highlighted in red dashed boxes in Figure 1.

**Visualization of FBNet output features.** To further show the validity of our proposed FBNet, we visualize some feature maps generated by FBNet in Figure 7. We can find that foreground targets like poles, traffic lights, trucks, people, motorcycles are all significantly strengthened in the high-level features. Meanwhile, stuff classes are suppressed to some extent. It satisfies our motivation because FBNet is designed as a feature modulator to enhance the deep representation of foreground classes.

Method	Conference	Backbone	mIoU(%)
NiseNet[36]	ICIP 2019	-	53.5
FasterSeg[8]	ICLR 2020	-	55.3
DeepLabv3+ [7]	ECCV 2018	ResNet-101	64.9
HANet[12]	CVPR 2020	ResNet-101	65.6
<b>Ours</b>	N/A	ResNet-101	<b>66.3</b>

Table 6. Performance comparisons on the BDD100K dataset, and all these results are based on the single scale without flipping testing strategy for a fair comparison.

## 5. Conclusions

In this paper, we delve into the essential reason that depresses the foreground targets segmentation performance in urban-scene parsing, which we call *Feature Camouflage*. To relieve the problem, a novel module named Feature Balance Networks(FBNet) is proposed, which is composed of two key components, i.e., Block-wise Binary Cross-Entropy (BwBCE) and Dual Feature Modulator(DFM). BwBCE loss intends to ease feature camouflage from a gradient balanced perspective. At the same time, DFM is designed to strengthen the deep representation of the foreground class in high-level features under the supervision of BwBCE. We



conduct extensive experiments to verify the effectiveness of our proposed method, and we achieve a new SOTA result on two challenging urban-scene benchmarks, i.e., Cityscapes and BDD100K.

## References

- [1] Vijay Badrinarayanan, Alex Kendall, and Roberto Cipolla. Segnet: A deep convolutional encoder-decoder architecture for image segmentation. *IEEE transactions on pattern analysis and machine intelligence*, 39(12):2481–2495, 2017. 3
- [2] Kaidi Cao, Colin Wei, Adrien Gaidon, Nikos Arachiga, and Tengyu Ma. Learning imbalanced datasets with label-distribution-aware margin loss. In *Advances in Neural Information Processing Systems*, pages 1567–1578, 2019. 2, 3
- [3] Nicolas Carion, Francisco Massa, Gabriel Synnaeve, Nicolas Usunier, Alexander Kirillov, and Sergey Zagoruyko. End-to-end object detection with transformers. In *European Conference on Computer Vision*, pages 213–229. Springer, 2020. 4
- [4] Nitesh V Chawla, Kevin W Bowyer, Lawrence O Hall, and W Philip Kegelmeyer. Smote: synthetic minority over-sampling technique. *Journal of artificial intelligence research*, 16:321–357, 2002. 2, 3
- [5] Liang-Chieh Chen, George Papandreou, Iasonas Kokkinos, Kevin Murphy, and Alan L Yuille. Deeplab: Semantic image segmentation with deep convolutional nets, atrous convolution, and fully connected crfs. *IEEE transactions on pattern analysis and machine intelligence*, 40(4):834–848, 2017. 3
- [6] Liang-Chieh Chen, George Papandreou, Florian Schroff, and Hartwig Adam. Rethinking atrous convolution for semantic image segmentation. *arXiv preprint arXiv:1706.05587*, 2017. 3
- [7] Liang-Chieh Chen, Yukun Zhu, George Papandreou, Florian Schroff, and Hartwig Adam. Encoder-decoder with atrous separable convolution for semantic image segmentation. In *Proceedings of the European conference on computer vision (ECCV)*, pages 801–818, 2018. 1, 2, 3, 6, 7, 8
- [8] Wuyang Chen, Xinyu Gong, Xianming Liu, Qian Zhang, Yuan Li, and Zhangyang Wang. Fasterseg: Searching for faster real-time semantic segmentation. *arXiv preprint arXiv:1912.10917*, 2019. 8
- [9] Wanli Chen, Xinge Zhu, Ruoqi Sun, Junjun He, Ruiyu Li, Xiaoyong Shen, and Bei Yu. Tensor low-rank reconstruction for semantic segmentation. In *European Conference on Computer Vision*, pages 52–69. Springer, 2020. 8
- [10] Yuhua Chen, Wen Li, and Luc Van Gool. Road: Reality oriented adaptation for semantic segmentation of urban scenes. In *Proceedings of the IEEE Conference on Computer Vision and Pattern Recognition*, pages 7892–7901, 2018. 3
- [11] Ho Kei Cheng, Jihoon Chung, Yu-Wing Tai, and Chi-Keung Tang. Cascadepsp: Toward class-agnostic and very high-resolution segmentation via global and local refinement. In *Proceedings of the IEEE/CVF Conference on Computer Vision and Pattern Recognition*, pages 8890–8899, 2020. 2
- [12] Sungha Choi, Joanne T Kim, and Jaegul Choo. Cars can’t fly up in the sky: Improving urban-scene segmentation via height-driven attention networks. In *Proceedings of the IEEE/CVF Conference on Computer Vision and Pattern Recognition*, pages 9373–9383, 2020. 3, 8
- [13] MMSegmentation Contributors. MMSegmentation: Openmmlab semantic segmentation toolbox and benchmark. <https://github.com/open-mmlab/mms Segmentation>, 2020. 4
- [14] Marius Cordts, Mohamed Omran, Sebastian Ramos, Timo Rehfeld, Markus Enzweiler, Rodrigo Benenson, Uwe Franke, Stefan Roth, and Bernt Schiele. The cityscapes dataset for semantic urban scene understanding. In *Proceedings of the IEEE conference on computer vision and pattern recognition*, pages 3213–3223, 2016. 1, 2, 3, 6
- [15] Yin Cui, Menglin Jia, Tsung-Yi Lin, Yang Song, and Serge Belongie. Class-balanced loss based on effective number of samples. In *Proceedings of the IEEE Conference on Computer Vision and Pattern Recognition*, pages 9268–9277, 2019. 2, 3
- [16] Henghui Ding, Xudong Jiang, Ai Qun Liu, Nadia Magnenat Thalmann, and Gang Wang. Boundary-aware feature propagation for scene segmentation. In *Proceedings of the IEEE International Conference on Computer Vision*, pages 6819–6829, 2019. 8
- [17] Chris Drummond. Class imbalance and cost sensitivity: Why undersampling beats oversampling. In *ICML-KDD 2003 Workshop: Learning from Imbalanced Datasets*, 2003. 2, 3
- [18] Jun Fu, Jing Liu, Haijie Tian, Yong Li, Yongjun Bao, Zhiwei Fang, and Hanqing Lu. Dual attention network for scene segmentation. In *Proceedings of the IEEE Conference on Computer Vision and Pattern Recognition*, pages 3146–3154, 2019. 7, 8
- [19] Haibo He, Yang Bai, Edwardo A Garcia, and Shutao Li. Adasyn: Adaptive synthetic sampling approach for imbalanced learning. In *2008 IEEE international joint conference on neural networks (IEEE world congress on computational intelligence)*, pages 1322–1328. IEEE, 2008. 2, 3
- [20] Kaiming He, Xiangyu Zhang, Shaoqing Ren, and Jian Sun. Deep residual learning for image recognition. In *Proceedings of the IEEE conference on computer vision and pattern recognition*, pages 770–778, 2016. 1, 6
- [21] Hanzhe Hu, Deyi Ji, Weihao Gan, Shuai Bai, Wei Wu, and Junjie Yan. Class-wise dynamic graph convolution for semantic segmentation. *arXiv preprint arXiv:2007.09690*, 2020. 8
- [22] Chen Huang, Yining Li, Change Loy Chen, and Xiaoou Tang. Deep imbalanced learning for face recognition and attribute prediction. *IEEE transactions on pattern analysis and machine intelligence*, 2019. 2, 3
- [23] Gao Huang, Zhuang Liu, Laurens Van Der Maaten, and Kilian Q Weinberger. Densely connected convolutional networks. In *Proceedings of the IEEE conference on computer vision and pattern recognition*, pages 4700–4708, 2017. 1
- [24] Zilong Huang, Xinggang Wang, Lichao Huang, Chang Huang, Yunchao Wei, and Wenyu Liu. Ccnet: Criss-cross

- attention for semantic segmentation. In *Proceedings of the IEEE International Conference on Computer Vision*, pages 603–612, 2019. 6, 7, 8
- [25] Tsung-Wei Ke, Jyh-Jing Hwang, Ziwei Liu, and Stella X Yu. Adaptive affinity fields for semantic segmentation. In *Proceedings of the European Conference on Computer Vision (ECCV)*, pages 587–602, 2018. 6, 8
- [26] Alex Krizhevsky, Ilya Sutskever, and Geoffrey E Hinton. Imagenet classification with deep convolutional neural networks. *Advances in neural information processing systems*, 25:1097–1105, 2012. 1
- [27] Xin Li, Zequn Jie, Wei Wang, Changsong Liu, Jimei Yang, Xiaohui Shen, Zhe Lin, Qiang Chen, Shuicheng Yan, and Jiashi Feng. Foveanet: Perspective-aware urban scene parsing. In *Proceedings of the IEEE International Conference on Computer Vision*, pages 784–792, 2017. 3
- [28] Xia Li, Yibo Yang, Qijie Zhao, Tiancheng Shen, Zhouchen Lin, and Hong Liu. Spatial pyramid based graph reasoning for semantic segmentation. In *Proceedings of the IEEE/CVF Conference on Computer Vision and Pattern Recognition*, pages 8950–8959, 2020. 8
- [29] Xiangtai Li, Houlong Zhao, Lei Han, Yunhai Tong, and Kuiyuan Yang. Gff: Gated fully fusion for semantic segmentation. *arXiv preprint arXiv:1904.01803*, 2019. 2
- [30] Guosheng Lin, Anton Milan, Chunhua Shen, and Ian Reid. Refinenet: Multi-path refinement networks for high-resolution semantic segmentation. In *Proceedings of the IEEE conference on computer vision and pattern recognition*, pages 1925–1934, 2017. 3
- [31] Tsung-Yi Lin, Piotr Dollár, Ross Girshick, Kaiming He, Bharath Hariharan, and Serge Belongie. Feature pyramid networks for object detection. In *Proceedings of the IEEE conference on computer vision and pattern recognition*, pages 2117–2125, 2017. 2
- [32] Songtao Liu, Di Huang, and Yunhong Wang. Learning spatial fusion for single-shot object detection. *arXiv preprint arXiv:1911.09516*, 2019. 2
- [33] Shu Liu, Lu Qi, Haifang Qin, Jianping Shi, and Jiaya Jia. Path aggregation network for instance segmentation. In *Proceedings of the IEEE conference on computer vision and pattern recognition*, pages 8759–8768, 2018. 2
- [34] Wei Liu, Andrew Rabinovich, and Alexander C Berg. Parsenet: Looking wider to see better. *arXiv preprint arXiv:1506.04579*, 2015. 6
- [35] Jonathan Long, Evan Shelhamer, and Trevor Darrell. Fully convolutional networks for semantic segmentation. In *Proceedings of the IEEE conference on computer vision and pattern recognition*, pages 3431–3440, 2015. 1, 3, 6
- [36] Sauradip Nag, Saptakatha Adak, and Sukhendu Das. What’s there in the dark. In *2019 IEEE International Conference on Image Processing (ICIP)*, pages 2996–3000. IEEE, 2019. 8
- [37] Gerhard Neuhold, Tobias Ollmann, Samuel Rota Buló, and Peter Kontschieder. The mapillary vistas dataset for semantic understanding of street scenes. In *Proceedings of the IEEE International Conference on Computer Vision*, pages 4990–4999, 2017. 7
- [38] Hyeonwoo Noh, Seunghoon Hong, and Bohyung Han. Learning deconvolution network for semantic segmentation. In *Proceedings of the IEEE international conference on computer vision*, pages 1520–1528, 2015. 3
- [39] Olaf Ronneberger, Philipp Fischer, and Thomas Brox. U-net: Convolutional networks for biomedical image segmentation. In *International Conference on Medical image computing and computer-assisted intervention*, pages 234–241. Springer, 2015. 3
- [40] Abhinav Shrivastava, Abhinav Gupta, and Ross Girshick. Training region-based object detectors with online hard example mining. In *Proceedings of the IEEE conference on computer vision and pattern recognition*, pages 761–769, 2016. 6
- [41] Jun Shu, Qi Xie, Lixuan Yi, Qian Zhao, Sanping Zhou, Zongben Xu, and Deyu Meng. Meta-weight-net: Learning an explicit mapping for sample weighting. In *Advances in Neural Information Processing Systems*, pages 1919–1930, 2019. 2
- [42] Karen Simonyan and Andrew Zisserman. Very deep convolutional networks for large-scale image recognition. *arXiv preprint arXiv:1409.1556*, 2014. 1
- [43] Ke Sun, Bin Xiao, Dong Liu, and Jingdong Wang. Deep high-resolution representation learning for human pose estimation. In *Proceedings of the IEEE/CVF Conference on Computer Vision and Pattern Recognition*, pages 5693–5703, 2019. 2
- [44] Christian Szegedy, Wei Liu, Yangqing Jia, Pierre Sermanet, Scott Reed, Dragomir Anguelov, Dumitru Erhan, Vincent Vanhoucke, and Andrew Rabinovich. Going deeper with convolutions. In *Proceedings of the IEEE conference on computer vision and pattern recognition*, pages 1–9, 2015. 1
- [45] Towaki Takikawa, David Acuna, Varun Jampani, and Sanja Fidler. Gated-scnn: Gated shape cnns for semantic segmentation. In *Proceedings of the IEEE/CVF International Conference on Computer Vision*, pages 5229–5238, 2019. 8
- [46] Ahmad S Tarawneh, Ahmad BA Hassanat, Khalid Almo-hammadi, Dmitry Chetverikov, and Colin Bellinger. Smote-funa: Synthetic minority over-sampling technique based on furthest neighbour algorithm. *IEEE Access*, 8:59069–59082, 2020. 2
- [47] Maoke Yang, Kun Yu, Chi Zhang, Zhiwei Li, and Kuiyuan Yang. Denseaspp for semantic segmentation in street scenes. In *Proceedings of the IEEE Conference on Computer Vision and Pattern Recognition*, pages 3684–3692, 2018. 3, 8
- [48] Changqian Yu, Jingbo Wang, Changxin Gao, Gang Yu, Chunhua Shen, and Nong Sang. Context prior for scene segmentation. In *Proceedings of the IEEE/CVF Conference on Computer Vision and Pattern Recognition*, pages 12416–12425, 2020. 6, 7, 8
- [49] Changqian Yu, Jingbo Wang, Chao Peng, Changxin Gao, Gang Yu, and Nong Sang. Bisenet: Bilateral segmentation network for real-time semantic segmentation. In *Proceedings of the European conference on computer vision (ECCV)*, pages 325–341, 2018. 4, 6, 7
- [50] Fisher Yu and Vladlen Koltun. Multi-scale context aggregation by dilated convolutions. *arXiv preprint arXiv:1511.07122*, 2015. 3, 6, 7, 8

- [51] Fisher Yu, Wenqi Xian, Yingying Chen, Fangchen Liu, Mike Liao, Vashisht Madhavan, and Trevor Darrell. Bdd100k: A diverse driving video database with scalable annotation tooling. *arXiv preprint arXiv:1805.04687*, 2(5):6, 2018. [1](#), [2](#), [3](#), [6](#)
- [52] Yuhui Yuan, Xilin Chen, and Jingdong Wang. Object-contextual representations for semantic segmentation. *arXiv preprint arXiv:1909.11065*, 2019. [6](#), [8](#)
- [53] Sergey Zagoruyko and Nikos Komodakis. Wide residual networks. *arXiv preprint arXiv:1605.07146*, 2016. [7](#)
- [54] Fan Zhang, Yanqin Chen, Zhihang Li, Zhibin Hong, Jingtuo Liu, Feifei Ma, Junyu Han, and Errui Ding. Acfnnet: Attentional class feature network for semantic segmentation. In *Proceedings of the IEEE International Conference on Computer Vision*, pages 6798–6807, 2019. [6](#), [7](#), [8](#)
- [55] Hang Zhang, Kristin Dana, Jianping Shi, Zhongyue Zhang, Xiaoang Wang, Amrbrish Tyagi, and Amit Agrawal. Context encoding for semantic segmentation. In *Proceedings of the IEEE conference on Computer Vision and Pattern Recognition*, pages 7151–7160, 2018. [3](#), [4](#)
- [56] Zhenli Zhang, Xiangyu Zhang, Chao Peng, Xiangyang Xue, and Jian Sun. Exfuse: Enhancing feature fusion for semantic segmentation. In *Proceedings of the European Conference on Computer Vision (ECCV)*, pages 269–284, 2018. [2](#)
- [57] Hengshuang Zhao, Jianping Shi, Xiaojuan Qi, Xiaoang Wang, and Jiaya Jia. Pyramid scene parsing network. In *Proceedings of the IEEE conference on computer vision and pattern recognition*, pages 2881–2890, 2017. [3](#), [4](#), [6](#), [7](#), [8](#)
- [58] Qijie Zhao, Tao Sheng, Yongtao Wang, Zhi Tang, Ying Chen, Ling Cai, and Haibin Ling. M2det: A single-shot object detector based on multi-level feature pyramid network. In *Proceedings of the AAAI conference on artificial intelligence*, volume 33, pages 9259–9266, 2019. [2](#)
- [59] Lanyun Zhu, Deyi Ji, Shiping Zhu, Weihao Gan, Wei Wu, and Junjie Yan. Learning statistical texture for semantic segmentation, 2021. [8](#)
- [60] Yi Zhu, Karan Sapra, Fitsum A Reda, Kevin J Shih, Shawn Newsam, Andrew Tao, and Bryan Catanzaro. Improving semantic segmentation via video propagation and label relaxation. In *Proceedings of the IEEE Conference on Computer Vision and Pattern Recognition*, pages 8856–8865, 2019. [3](#)
- [61] Yang Zou, Zhiding Yu, BVK Kumar, and Jinsong Wang. Unsupervised domain adaptation for semantic segmentation via class-balanced self-training. In *Proceedings of the European conference on computer vision (ECCV)*, pages 289–305, 2018. [2](#), [3](#)